JOURNAL OF MATERIALS SCIENCE **39** (2004) 7145–7152

Modelling of the arc plasma behaviour in the VAR process

P. CHAPELLE, H. EL MIR, J. P. BELLOT, A. JARDY, D. ABLITZER
Laboratoire de Science et Génie des Matériaux et de Métallurgie (UMR 7584), Ecole des Mines, Parc de Saurupt, 54042 Nancy Cedex, France
E-mail: chapelle@mines.inpl-nancy.fr

D. LASALMONIE
Centre de Recherches de la Compagnie Européenne du Zirconium CEZUS, 73403 Ugine Cedex, France

As part of a complete theoretical description of the behaviour of the electric arc in the vacuum arc remelting process, a model has been developed for the column of plasma generated by a single cluster of cathode spots. The model combines a kinetic approach, taking into account the formation of the plasma in the cathodic region, and a hydrodynamic approach, describing the expansion of the plasma in the vacuum between the electrodes. The kinetic model is based on a system of Boltzmann-Vlasov-Poisson equations and uses a particle-type simulation procedure, combining the PIC (Particle In Cell) and FPM (Finite Point Set Method) methods. In the two-dimensional hydrodynamic model, the plasma is represented as a mixture of two continuous fluids (the electrons and the ions), each described by a system of coupled transport equations. Finally, a simplified method has been defined for calculating the electric current density and the energy flux density transmitted by the plasma to the anode. In order to achieve complete modelling of the electric arc in the VAR furnace, the movement of all the clusters on the cathode surface has been simulated, based on a detailed experimental study performed on industrial plant. The results of the numerical simulation presented are consistent with a certain number of experimental results available in the literature. In particular, the model predicts a percentage of the electric power of the arc transmitted to the anode (25%) in good agreement with the value indicated in the literature.

1. Introduction

Among the secondary steelmaking techniques, the VAR (Vacuum Arc Remelting) process consists of remelting a consumable electrode with the aid of an electric arc. This operation ensures both the purification of the metal as it is gradually melted, and controlled solidification of the ingot in terms of structure and chemical homogeneity. The VAR process is employed for the manufacturing of reactive metals (titanium and zirconium), and for the production of nickel-base alloys, special steels, and refractory metals.

An electric arc, which provides the energy necessary to melt the alloy, is maintained between the tip of the consumable electrode (cathode) and, at the start of the operation, the bottom of the water-cooled copper mould, and later, the top of the secondary ingot (anode), which is gradually built up in the mould (Fig. 1). The ingot solidifies in contact with the mould walls. The electric arc plays a predominant role in the VAR process. In particular, by affecting the distribution of energy and electric current at the surface of the melt pool, the behaviour of the arc influences the ingot solidification conditions, and therefore the quality of the final product.

Knowledge of the electric arc in the VAR process is based on experimental studies performed by Zanner and co-workers (e.g. [1, 2]) in the 1980s on remelting of nickel- and iron-based alloy electrodes. Similar experiments have been carried out more recently by the present authors, in collaboration with the CEZUS company, on zirconium alloy electrodes [3]. The main conclusions from these observations are that the behaviour of the electric arc in the VAR process is similar to the diffuse mode of a vacuum arc created between cold solid electrodes for the same range of current densities. The arc consists of several dispersed clusters of cathode spots moving erratically over the whole surface of the cathode. Each spot is a highly luminous region, which produces a plasma jet expanding under vacuum in the electrode gap. A diffuse glow fills the interelectrode gap and the anode remains non luminous.

The only attempts to model the electric arc in the VAR process are global models, which do not describe the complex processes governing the arc plasma

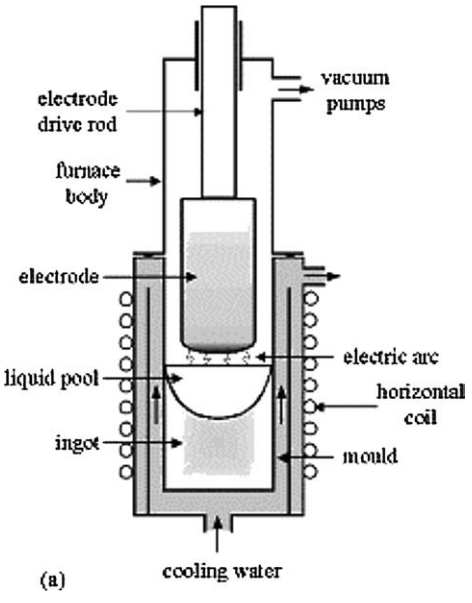

Figure 1 Schematic principle of the VAR process.

behaviour. Zanner *et al*. [4] and Jardy *et al*. [5] have used global energy balances of the remelting operation to study the distribution of the arc power in the furnace. Williamson *et al*. [6] have treated the arc as a collection of independent clusters and represented the plasma column emitted by each cluster as an ohmic conductor, whose behaviour is governed by Ohm's law.

The mathematical model described in the present article aims to precisely calculate the distributions of thermal energy and electric current transferred to the surface of the melt pool (anode). A complete description of the column of plasma generated by a unique cluster of cathode spots is presented. It combines two approaches, one kinetic and the other hydrodynamic, which account for the emission and ionization of metallic vapour particles at the cathode and their expansion in the electrode gap. In order to achieve complete modelling of the electric arc in the VAR process, the motion of all the clusters on the cathode surface is then modelled, based on a detailed experimental study of cluster displacement in an industrial VAR furnace.

2. Methodology

The experimental observations [3] completed by data available in the literature [7, 8] reveal in the electron emission zones a complex self-similar structure including three length scales. A cathode spot has a radius of about 200 μm and is composed on average of about ten distinct emissive sites called "micro-spots," whose radius is of the order of 10 μm. In turn, groups of about ten spots form "clusters" with a radius of the order of 1.5 mm. The basic assumption employed was therefore that the arc can be represented as a collection of identical independent clusters, each composed of one hundred micro-spots. Neglecting the interactions between individual clusters seems reasonable, since according to video observations [3], for most of the time, the clusters (with a radius of the order of 1.5 mm) are scattered over the whole surface of the cathode (whose radius is of the order of ten centimetres). Of course, although the hydrodynamic interactions are ignored, the electromagnetic interactions between clusters will be handled. This representation of the arc enables the study to be initially limited to the behaviour of a single cluster considered to be motionless. Indeed each micro-spot, and therefore the complete cluster, can be studied in the quasi-stationary regime, since the velocity of the plasma jet ($\sim 10^4$ m/s [7]) is much greater than the displacement speed of the emissive sites ($\sim$1–10 m/s). The model of a single cluster is then combined with a model of the motion of all the clusters at the cathode surface in order to obtain a complete description of the electric arc behaviour in the VAR process.

The modelling of the plasma column generated by a single cluster combines two models, as shown in Fig. 2.

– The first model describes the cathodic region adjacent to each micro-spot, including the cathodic space charge sheath and the ionization zone. In this region (whose length is of the order of 1–10 μm [7]) the particle density and temperature gradients are so large that a kinetic model is necessary.

– The second model treats the plasma expansion region using a hydrodynamic approach. In this region, the low particle densities (the jet expands under

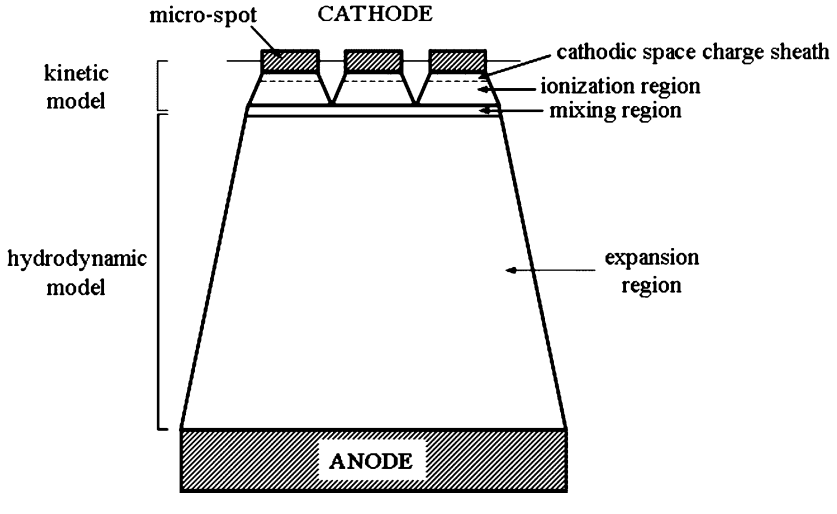

Figure 2 Schematic description of the plasma column emitted by a cluster.

vacuum) and the relatively low energy of the electrons (which have become thermal) justify the assumption that ionization and recombination phenomena can be neglected.

Finally, the modelling of the region of mixing (assumed to be very thin) weakly couples the kinetic and hydrodynamic models. It defines the characteristic parameters of the plasma in the entry section of the expansion region, based on the characteristic parameters of the plasma jets emitted by all of the micro-spots.

The following sections outline the main characteristic of each model. A detailed presentation of the kinetic and hydrodynamic models and the associated numerical solution techniques can be found in [9].

3. Kinetic model

The plasma is composed of several types of particles, including neutral species (o), ions (i) with different degrees of ionization, and electrons (e). The modelling of the plasma behaviour is based on a system of kinetic Equations 1, which combines the Vlasov's equation describing the transport of the charged particles under the effect of a self-consistent electric field, the Poisson's equation defining the electric field, and the Boltzmann operator, which accounts for the interactions between particles:

$$\frac{\partial f_s}{\partial t} + \vec{v}\frac{\partial f_s}{\partial \vec{x}} + \frac{q_s}{m_s}\vec{E}\frac{\partial f_s}{\partial \vec{v}} = \sum_r Q_{r,s} + J_s^{I,R} \qquad \frac{\partial}{\partial \vec{x}}\vec{E} = \frac{e}{\varepsilon_0}(n_i - n_e) \tag{1}$$

where $f_s(\vec{x}, \vec{v}, t)$ is the velocity distribution function for the particles of species s, $\vec{E}$ is the electric field and n_s is the density of particles of species s.

Via Boltzmann operators, the $Q_{r,s}$ terms express the individual effects due to binary elastic collisions. This approach is rigorous for the short range interactions between neutral particles and for the interactions between neutral and charged particles. However, the same formalism has been conserved to describe the longer range interactions between charged particles, by using appropriately adapted effective collision cross sections [10, 11]. In order to model ionization and recombination processes ($J_s^{I,R}$), the Boltzmann operator was generalized using the formalism of Kuscer [12] to include multiple inelastic collisions. Only the phenomena involving ionization by electron impact are modelled, since the electrons are much more mobile than the neutral species and ions. The ionization and recombination reactions considered can be written respectively:

$$M^{Z+} + e^- \longrightarrow M^{(Z+1)+} + 2e^- \tag{2}$$

$$M^{(Z+1)+} + 2e^- \longrightarrow M^{Z+} + e^- \tag{3}$$

The Boltzmann-Vlasov-Poisson system requires the definition of boundary conditions at the beginning of the expansion region (Fig. 2). Since the two models are not coupled, there is in principle no data of the hydrodynamic simulation of the expansion region that can be used to define these boundary conditions. Conditions were therefore chosen corresponding to an imaginary anode, thus defining the electrical potential and the velocity distribution functions for each particle species. Only two-way coupling at the common boundary between the kinetic and hydrodynamic models will enable these boundary conditions to be avoided in the future. Neutral particles at the cathode are considered to be emitted by an evaporation process. The absence of emission and reflection of ions is assumed at the electrodes, all the ions being created by ionization within the plasma. In the cathode spot, the distribution of the emitted electrons is given by a semi-Maxwell function.

A particle method is used for the numerical simulation of the system of Equations 1. The system is dissociated into a Vlasov-Poisson system and a homogeneous system of Boltzmann equations.

$$\frac{\partial f_s}{\partial t} = -\vec{v}\frac{\partial f_s}{\partial \vec{x}} - \frac{q_s}{m_s}\vec{E}\frac{\partial f_s}{\partial \vec{v}} \tag{4}$$

$$\frac{\partial}{\partial \vec{x}}\vec{E} = \frac{e}{\varepsilon_0}(n_i - n_e) \tag{5}$$

$$\frac{\partial f_s}{\partial t} = \sum_r Q_{r,s} + J_s^{I,R} \tag{6}$$

For each time interval, the Vlasov-Poisson system (Equations 4 and 5) is simulated using the PIC (Particle In Cell) method, and the Boltzmann Equations 6 are then simulated by the FPM (Finite Point Set Method) method. When an established flow regime is attained, the macroscopic parameters (density, velocity and temperature) relative to each species can be calculated in each mesh cell by averaging the appropriate microscopic parameters.

4. Hydrodynamic model

The hydrodynamic model of the axisymmetric plasma expansion is based on the following assumptions, which have been formulated from the results of the kinetic model at the exit of the cathodic region. The plasma treated as totally ionized and electrically neutral is represented as a mixture of two continuous fluids: the electrons and the ions characterized by a mean positive charge (Z_i). The plasma composition remains unchanged during its expansion, since collisions involving ionization or recombination are relatively improbable and can therefore be neglected. Radiative phenomena are disregarded [13]. It can be readily verified that the terms representing viscous forces and heat conduction in the transport equations for the ions and those corresponding to viscous and inertial forces in the transport equations for the electrons are negligible [14]. Moreover, it is also reasonable to neglect the conduction term in the energy transport equation for the electrons [15].

Hence, the two systems of conservation equations describing the flows of ions and electrons reduce to:

Ions:

$$\nabla \cdot (n_i \vec{u}_i) = 0 \quad (7)$$

$$\nabla \cdot (m_i n_i \vec{u}_i \vec{u}_i) = -Z_i e n_i \vec{\nabla}\phi - \vec{\nabla}(n_i k T_i) + \vec{R}_{ie} \quad (8)$$

$$\nabla \cdot \left(\frac{3}{2} n_i \vec{u}_i k T_i\right) = -n_i k T_i \nabla \cdot \vec{u}_i - \vec{R}_{ie} \cdot \vec{u}_i + Q_{ie} \quad (9)$$

Electrons:

$$0 = e n_e \vec{\nabla}\phi - \vec{\nabla}(n_e k T_e) + \vec{R}_{ei} \quad (10)$$

$$\nabla \cdot \left(\frac{3}{2} n_e \vec{u}_e k T_e\right) = -n_e k T_e \nabla \cdot \vec{u}_e - \vec{R}_{ei} \cdot \vec{u}_e + Q_{ei} \quad (11)$$

Furthermore, the electrical potential must obey Poisson's equation:

$$\nabla^2 \phi = 0 \quad (12)$$

In the Equations 8–11, the terms $\vec{R}_{ei}$ and $\vec{R}_{ie}$ (respectively Q_{ei} and Q_{ie}) describe the exchanges of momentum (respectively energy) during electron-ion collisions [16].

To facilitate the solution of the equation system (7)–(12), it is useful to add together the corresponding members of Equations 8 and 10. Taking into account the electrical neutrality of the plasma ($n_e = Z_i n_i$) and the property $\vec{R}_{ei} = -\vec{R}_{ie}$, this gives the equation:

$$\nabla \cdot (m_i n_i \vec{u}_i \vec{u}_i) = -\vec{\nabla}(n_i k T_i + n_e k T_e) \quad (13)$$

Furthermore, it is assumed that the ratio between the electronic and ionic currents remains constant at any points in the plasma. Because of the electrical neutrality, the velocities of the electrons and ions are then related by an equation of the type: $\vec{u}_e = \beta \vec{u}_i$, where β is a proportionality coefficient determined from the results of the kinetic calculation. This rough assumption, which avoids the need to solve the momentum transport equation for the electrons, gives acceptable results for a first approximation, as demonstrated in Section 6.

Finally, the set of equations describing the plasma can be reduced to Equations 7, 9, 11, 12 and 13, which form a perfectly determined system with 5 unknowns: n_i, $\vec{u}_i$, T_i, T_e and ϕ. A finite volume method has been employed to solve this system numerically.

The coupling of the kinetic and hydrodynamic models in the entry section of the expansion region considers that the intermediate mixing region is very thin and that there is no effect of mixing on the characteristic parameters of the plasma emitted by each of the micro-spots. The characteristic parameters of the plasma formed by combination of the plasma jets emitted by the 100 micro-spots are assumed to be uniform throughout the entry section of the expansion zone and are related to the characteristic parameters of the plasma emitted by a micro-spot by the following equations:

$$n_{i,2} = 100\,(S_1/S_2)\,n_{i,1}, \quad \vec{u}_{i,2} = \vec{u}_{i,1},$$
$$T_{i,2} = T_{i,1}, \quad T_{e,2} = T_{e,1}, \quad \phi_2 = \phi_1 \quad (14)$$

where the indices 1 and 2 refer respectively to the exit section of the cathodic region and the entry section of the expansion region. S_i is the surface area of the section of index i. As regards the ion density, it is considered that the densities due to the 100 plasma jets simply add together. The joining procedure defined in this way ensures the continuity of the different fluxes of matter, momentum and energy.

The potential drop in the anode region is evaluated from the condition of continuity of the electronic current density at the boundary between the expansion and the anodic regions [17]. For the axial component, this condition can be written:

$$J_e = (J_{d,e} + J_{th,e}) \exp\left(\frac{eU_a}{kT_e}\right) \quad (15)$$

where U_a is the drop in anodic potential. On the right hand side, the density of the electronic current collected at the anode surface is the sum (weighted by $\exp(eU_a/kT_e)$) of a macroscopic current density ($J_{d,e}$) and a current density due to the thermal agitation of the electrons ($J_{th,e}$), defined respectively by the relations:

$$J_{d,e} = -e n_e u_e \quad \text{and} \quad J_{th,e} = -\frac{1}{4} e n_e \left(\frac{8kT_e}{\pi m_e}\right)^{1/2} \quad (16)$$

The energy flux density transmitted to the anode by the electrons and the ions can be expressed in the form:

$$P_\alpha = (J_\alpha/q_\alpha)\, W_\alpha \quad (\alpha = e, i) \quad (17)$$

where q_α and W_α are respectively the charge and the mean total energy for a particle of species α.

The mean energy transported by an electron is given by:

$$W_e = \frac{5}{2} k T_e + \frac{1}{2} m_e u_e^2 + e U_a + e U_s \quad (18)$$

The right hand side terms represent respectively the enthalpy of the electron, its kinetic energy, the kinetic energy lost in the anodic potential drop and the energy of extraction from the metal (U_s), ceded to the anode during capture of the electron.

The mean energy transported by an ion is given by:

$$W_i = \frac{5}{2} k T_i + \frac{1}{2} m_i u_i^2 + Z_i e U_a + U_r + L_v \quad (19)$$

The right hand side terms represent respectively the enthalpy of the ion, its kinetic energy, the kinetic energy received in the anodic potential drop, the energy of recombination of the ion at the anode surface ($U_r = \sum_{Z=1,2,..} f_Z U_Z - Z_i e U_s$, where U_Z is the ionization energy of ions of charge Z) and the latent heat of condensation of the ion (L_v).

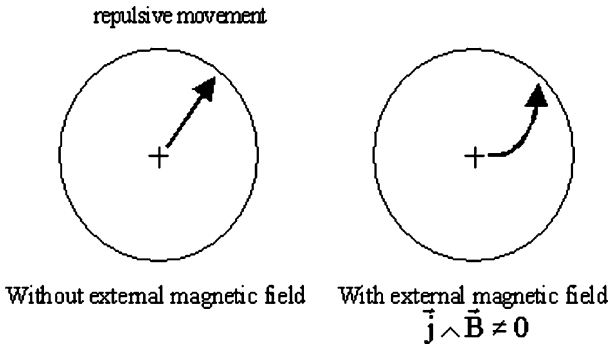

Figure 3 Schematic motion of the clusters without or with external magnetic field.

5. Model of the cluster motion on the cathode surface

A detailed study of the literature [18–20] and many trials of observation using an industrial VAR furnace have highlighted the main behaviour of the cathodic clusters in terms of trajectories, velocities and life time. Without any external magnetic field, the clusters move preferentially towards the periphery of the electrode following a radial displacement (see Fig. 3). In a magnetic field parallel to the cathode surface, cathode clusters in a vacuum arc move opposite to the Lorentz force vector ($\vec{j} \wedge \vec{B}$, i.e., the motion is retrograde). In that case, the two motions combine and the trajectories are curved as it is shown on the Fig. 3. The parameters such as the mean dwell time and the mean velocity have also been evaluated from high speed video camera recording as a function of the operating arc parameters [21].

We have developed a statistical numerical model of displacement of clusters. From a random initial location of the cluster, it describes the radial movement (if $\vec{j} \wedge \vec{B} = \vec{0}$) or the combined radial and orthoradial movement (if $\vec{j} \wedge \vec{B} \neq \vec{0}$). An example of trajectories of ten clusters is given in Fig. 4.

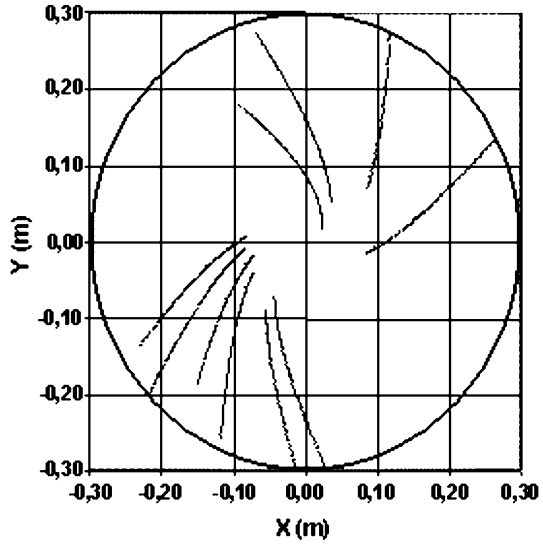

Figure 4 Example of trajectories simulated.

TABLE I Input parameters of the simulations

Parameter	Value	Reference
Distance cathode-anode	1.5 cm	[14]
Arc voltage	27 V	[14]
Current emitted by a cluster	380 A	[14]
Number of micro-spots in a cluster	100	[14]
Diameter of a cluster	$2R_0 = 3$ mm	[14]
Diameter of a micro-spot	20 μm	[14]
Mean ion charge in the expansion region (Z_i)	1.87	[14]
Ratio between the electronic and ionic currents in the expansion region (β)	20.04	[14]

Due to a lack of available data relative to the parameters of zirconium vacuum arcs in the literature, we have used the values reported for cathodes of titanium, whose properties are similar to those of zirconium.

6. Numerical results—Discussions

The simulation input parameters, which are given in Table I, combine experimental measurements, performed during the vacuum arc remelting of a zirconium alloy [14], and general data describing a cluster taken from the literature concerning arcs struck under vacuum between two cold solid electrodes [8].

6.1. Cathodic region adjacent to a micro-spot

An "imaginary" anode was placed at a distance of 4 μm from the cathode. Since the distance between the cathode and the "imaginary" anode is smaller than the micro-spot diameter, the simulation is performed in a one dimensional geometry. Fig. 5 shows the axial variations of the electrical potential and the space charge in the electrode gap. The variations in electrical potential and space charge are confined within two thin regions ($\sim$0.15 μm) immediately adjacent to the two electrodes, whereas, in the central region occupying most the electrode gap, the potential is essentially constant and the plasma is electrically neutral. The potential drop in the cathodic region ($\sim$47 V) is much higher than the total potential drop between the electrodes ($\sim$27 V). This is in qualitative agreement with several numerical results of the literature [22], showing the existence of a maximum electrical potential in the vicinity of the cathode ($\sim$5–15 V with respect to the anode potential).

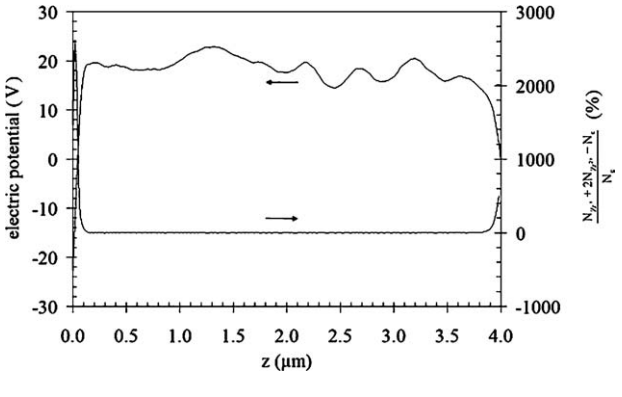

Figure 5 Electric potential and space charge, calculated by the kinetic model, as a function of the axial distance from the cathode. A fictitious anode has been set at a distance of 4 μm from the cathode.

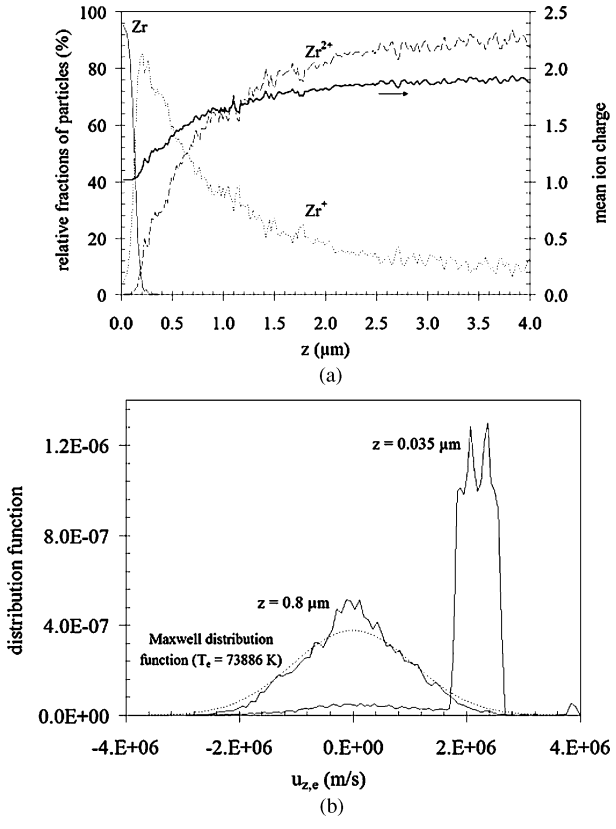

Figure 6 (a) Calculated plasma composition as a function of the axial distance from the cathode. (b) Electron axial velocity distribution function, calculated by the kinetic model, at two distances from the cathode. The broken curve corresponds to the Maxwell distribution function for the electron temperature ($T_e = 73886$ K).

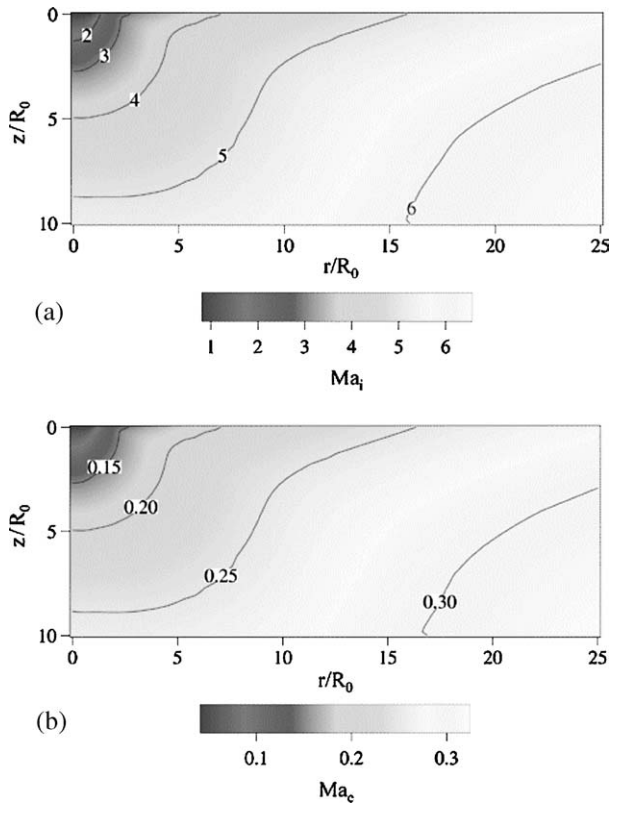

Figure 7 Field in r-z plane of (a) the ion Mach number and (b) the electron Mach number.

The variations of the plasma composition with the axial distance from the cathode surface are presented in Fig. 6a. The atoms of zirconium emitted at the cathode are rapidly ionized near the cathode surface. The plasma is completely ionized beyond a distance of about 0.4 μm from the cathode. This result is in good agreement with the very strongly ionized nature of vacuum arc plasmas reported in the literature [23]. The mean ion charge of the plasma increases up to a distance from the cathode of about 2.5 μm, then maintains a constant value of approximately 1.87. It can therefore be considered that the composition of the plasma is no longer modified beyond 2.5 μm. The ionization of zirconium particles is associated with the relaxation of the flux of electrons emitted at the cathode and accelerated through the cathodic potential drop. The relaxation of the electrons is illustrated in Fig. 6b, which shows the transition of the electron velocity distribution function from a function characterizing a beam of iso-energy particles in the acceleration region ($z = 0.035$ μm) to a Maxwell equilibrium function at a distance of 0.8 μm from the cathode.

In this example, it has been chosen to connect the hydrodynamic model to the kinetic model in the section located at 2.5 μm from the cathode. Indeed, the kinetic simulation predicts that the relaxation of each species (ions and electrons) towards a state close to the local thermodynamic equilibrium is complete beyond this point. However, comparison of the ionic and electronic temperature profiles (not shown here) indicates that the ions and electrons have not attained temperature equilibrium, requiring the use of a two-fluid hydrodynamic model. Moreover, at a distance further than 2.5 μm downstream from the cathode, the plasma is totally ionized ($Z_i = 1.87$) and electrically neutral and its composition remains constant, justifying several of the assumptions made in the hydrodynamic model (see Section 4). Finally, the kinetic calculation provides a value for the coefficient β (defined in Section 4) of 20.04, which reasonably agrees with the values (ranging from 11 to 41 depending on the current and the cathode material) reported in the literature [24, 25].

6.2. Expansion region

The hydrodynamic calculation at the entry of the expansion region uses the results of the kinetic calculation obtained at a distance of 2.5 μm from the cathode, taking into account the intermediate mixing region with the aid of the relations (14). The data necessary for the hydrodynamic model at the entry of the expansion region are as follows: $n_i = 3.52 \times 10^{21}$ m^{-3}, $u_{i,z} = 2314$ m/s, $T_i = 3360$ K, $T_e = 72233$ K, $\phi = 15$ V, $Z_i = 1.87$, $\beta = 20.04$.

Distributions in the r-z plane of the Mach number characterizing respectively the ion flow ($Ma_i = u_i/c_{s,i}$, where $c_{s,i} = (5k(T_e + T_i)/3m_i)^{1/2}$ is the sound velocity for the ion flow) and the electron flow ($Ma_e = u_e/c_{s,e}$, where $c_{s,e} = (5kT_e/3m_e)^{1/2}$ is the sound velocity for the electron flow) are shown in Fig. 7. The plasma expansion is accompanied by an important acceleration of the ion. The Mach number at the symmetry axis reaches a value of 5, corresponding to an ion velocity greater than 10^4 m/s. Note that the supersonic ion flow regime is

in agreement with experimental results reported in the literature [23]. From the momentum transport Equation 8, the acceleration of the ions is due to the combined effects of the forces associated respectively with the electric field, the ion pressure gradient and friction between the electrons and the ions. The electron-ion friction plays a predominant role and is responsible for more than 70% of the ion acceleration. The forces due to the electric field and the ionic pressure gradient have a secondary influence and are responsible respectively for 24 and 3% of the ion acceleration. Comparison of these percentages with those calculated by Hantzsche [26] (equal to 55, 15 and 30% respectively for the effects of electron-ion friction, the electric field and the pressure gradient) shows good qualitative agreement as regards the predominance of the effect of electron-ion friction. However, Hantzsche predicts a greater effect of the pressure gradient than that forecast by the present simulation.

Since the density and velocity of the electrons are assumed to be proportional to the density and velocity of the ions respectively, like the ions, the electrons undergo an expansion. This results in an increase in the Mach number characterizing the electron flow, which reaches a value close to 0.3 along the symmetry axis. The electron acceleration is due to the influence of the electron pressure gradient. The electric field (positive) and the electron-ion friction both tend to slow down the electrons. The electron flow regime remains subsonic at all points. The order of magnitude of the Mach numbers obtained is in agreement with values of the literature [26].

6.3. Energy flux density transmitted by a single cluster to the anode

The total energy flux density transmitted by a single cluster to the anode decreases rapidly with distance from the symmetry axis (Fig. 8). Integration of the total power transmitted by the plasma jet to the anode gives a value equal to 2567 W, representing a relative fraction of the electric power of the cluster (~10260 W) equal to 25%. This percentage is in good agreement with the order of magnitude of the fraction of the electric arc power transmitted to the anode in the VAR process, estimated in the literature from an overall energy balance

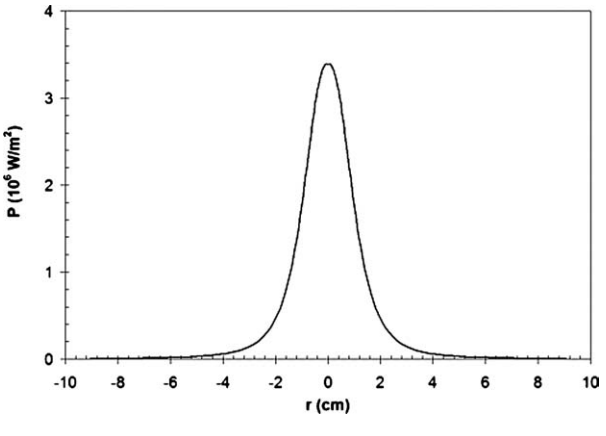

Figure 8 Distribution at the anode surface of the energy flux density supplied by the plasma jet emitted by a single cluster.

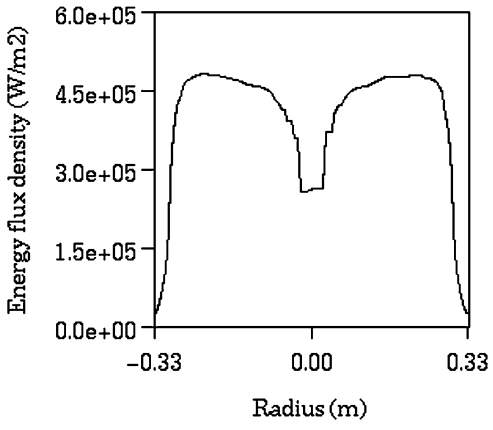

Figure 9 Distribution of energy flux density at the top of the ingot.

[5]. It should be realized that this power of 2567 W represents only the interaction between the plasma and the anode surface. It obviously does not include the enthalpy of the metal droplets that feed the anodic melt pool, nor the radiant heat exchanges between the surfaces of the anode, the cathode and the walls of the ingot mould.

6.4. Total energy flux density transmitted to the anode

Combining the model of cluster trajectories on the cathode surface with the energy flux density transmitted by a single cluster to the anode, the distribution of flux of energy on the overall surface of the ingot top can be easily calculated. An example of the results is given in Fig. 9, where the total intensity of the arc is 21 kA and the ingot diameter is 0.66 m. This top-hat profile is characteristic of the energy power distribution provided by the arc plasma at the top of the ingot. However we notice a depletion of power nearby the symmetry axis due to the radial direction of the cluster velocity. The magnitude of this depletion mainly depends on the life time of the clusters and the diameter of the electrode. This energy flux density profile provides of course the boundary condition for the computational software SOLAR developed at the Ecole des Mines de Nancy [27, 28].

7. Conclusions

A complete mathematical model of the electric arc plasma behaviour in the VAR process has been presented. It combines a model of the column of plasma generated by a single cluster of cathode spots with a description of the movement of all the clusters on the cathode surface. For the modelling of a single cluster, the formation of the plasma in the cathodic region is described using a kinetic approach, while the expansion of the plasma in the vacuum between the electrodes is treated by means of a two-fluid hydrodynamic model. A dynamic simulation of the trajectories of all the clusters on the cathode surface accounts of the combined effects of two types of motion of the clusters: a repulsive motion and a non retrograde motion in the opposite direction of the Lorentz forces. The velocity of each type of motion has been calculated under different operating conditions based on experimental observations.

The results of the numerical simulation, applied to the case of an arc created between two zirconium electrodes, correctly reproduce the important phenomena governing the formation and flow of the plasma. The kinetic calculation show that the plasma is very rapidly fully ionized and that its composition becomes frozen in the immediate vicinity of the cathode. In conformity with results published in the literature, the hydrodynamic model predicts that friction effects between the electrons and ions play a predominant role in the acceleration of the plasma jet. The models enable the calculation of the distributions of the electric current density and energy flux density transferred by the plasma to the surface of the anodic melt pool. The presented numerical results reveal that these distributions are axisymmetric with an off-centre maximum. The predicted percentage of the electric power of the arc transmitted to the anode ($\sim$25%) is in good agreement with the value reported in the literature. In the future, the distributions of energy and electric current obtained at the surface of the melt pool should be implemented as boundary conditions at the top surface of the ingot in the computational software SOLAR [27, 28] which simulates the hydro-thermo-chemical behaviour of the ingot.

References

1. F. J. ZANNER, *Met. Trans. B* **10B** (1979) 133.
2. R. L. WILLIAMSON and F. J. ZANNER, in Proceedings of the Vac. Met. Conf. on Melting and Processing of Specialty Materials, Warrendale, Pennsylvania, 1991, edited by N. Bhat, E. N. Bloore and D.R. Malley (Iron and Steel Society, 1992) p. 87.
3. P. CHAPELLE, J. P. BELLOT, A. JARDY, T. CZERWIEC, X. ROBBE, B. CHAMPIN and D. ABLITZER, *High Temp. Mater. Proc.* **4**(4) (2000) 493.
4. F. J. ZANNER and L. A. BERTRAM, Sandia National Laboratories, Report SAND 80-1156 (1980).
5. A. JARDY, L. FALK and D. ABLITZER, Mémoires et Etudes Scientifiques-Revue de Métallurgie (1991) p. 781.
6. R. L. WILLIAMSON, F. J. ZANNER and S. M. GROSSE, *Met. Trans. B* **28B** (1997) 1.
7. G. A. LYUBIMOV and V. I. RAKHOVSKII, *Sov. Phys. Usp.* **21**(8) (1978) 693.
8. P. SIEMROTH, T. SCHÜLKE and T. WITKE, *IEEE Trans. Plasma Sci.* **25**(4) (1997) 571.
9. P. CHAPELLE, J. P. BELLOT, H. DUVAL, A. JARDY and D. ABLITZER, *J. Phys. D: Appl. Phys.* **35** (2002) 137.
10. Y. WENG and M. J. KUSHNER, *Phys. Rev. A* **42**(10) (1990) 6192.
11. M. YOUSFI, A. HIMOUDI and A. GAOUAR, *ibid.* **46**(12) (1992) 7889.
12. I. KUSNER, *Physica A* **176** (1991) 542.
13. A. ANDERS and S. ANDERS, *J. Phys. D: Appl. Phys.* **24** (1991) 1986.
14. P. CHAPELLE, Etude expérimentale et modélisation de l'arc électrique dans le procédé de refusion VAR, PhD thesis, INPL (2001).
15. C. WIECKERT, *Contrib. Plasma Phys.* **27**(5) (1987) 309.
16. V. E. GOLANT, A. P. ZHILINSKY and I. E. SAKHAROV, "Fundamentals of Plasma Physics" (Wiley, New York, 1980).
17. C. WIECKERT and W. EGLI, *IEEE Trans. Plasma Sci.* **17**(5) (1989) 649.
18. B. JUTTNER, *J. Phys. D: Appl. Phys.* **34** (2001) 103.
19. S. A. BARENGOLTS *et al.*, *Techn. Phys.* **43**(6) (1998) 668.
20. B. Y. MOIZHES and V. A. NEMCHINSKII, *Soviet Techn. Phys. Lett.* **5**(2) (1979) 78.
21. H. ELMIR, J. P. BELLOT and A. JARDY, Mouvement des clusters de spots à la surface de la cathode, Internal Report Cezus (2002).
22. I. I. BEILIS, in "Handbook of Vacuum Arc Science and Technology," edited by R. L. Boxman, P. J. Martin and D. M. Sanders (Noyes Publications, New Jersey, 1995) p. 208.
23. R. L. BOXMAN, S. GOLDSMITH and A. GREENWOOD, *IEEE Trans. Plasma Sci.* **25**(6) (1997) 1174.
24. C. W. KIMBLIN, *J. Appl. Phys.* **44**(7) (1973) 3074.
25. Z. ZALUCKI and J. KUTZNER, in Proceedings of the 7th Int. Symp. Dis. and Elect. Insul. in Vac., Nobosibirsk, USSR, 1976, p. 297.
26. E. HANTZCHE, *J. Phys. D: Appl. Phys.* **24** (1991) 1339.
27. A. F. WILSON, A. JARDY and S. P. FOX, in Proceedings of the 2003 International Symposium on Liquid Metal Processing and Casting, Nancy, edited by P. D. Lee, A. Mitchell, J. P. Bellot and A. Jardy, Sept. 2003, p. 11.
28. T. QUATRAVAUX, S. RYBERON, S. HANS, A. JARDY, B. LUSSON, P. E. RICHY and D. ABLITZER, *J. Mater. Sci.* (in this issue) (2004).

Received 10 March
and accepted 14 June 2004